High-speed optical coherence tomography imaging with a tunable HCG-VCSEL light source at the 1060nm wavelength window

Ting-Yen Tsai[a], Ting-Hao Chen[a], Hung-Kai Chen[b], Chuan-Bor Chueh[a], Dalila Ellafi[b], Chris Chase[b], Hao-Chung Kuo[e], Meng-Tsan Tsai[c, d], Michael C. Y. Huang[b], and Hsiang-Chieh Lee*[a, f]

[a]Graduate Institute of Photonics and Optoelectronics, National Taiwan University, 2Taipei, 106, Taiwan; [b] Bandwidth10 LTD. Berkeley, CA, USA, 94704; [c]Department of Electrical Engineering, Chang Gung University, Taoyuan, 333, Taiwan; [d]Department of Neurosurgery, Chang Gung Memorial Hospital, Linkou, 244, Taiwan; [e]Department of Photonics, National Yang Ming Chiao Tung University, Hsinchu, 300, Taiwan; [f]Department of Electrical Engineering, National Taiwan University, Taipei, 106, Taiwan

ABSTRACT

We present a high-speed swept-source optical coherence tomography (SS-OCT) imaging system using an electrically-pumped, micro-electromechanical (MEMS) tunable HCG-VCSEL operating at the 1060 nm wavelength regime. Comparing to existing MEMS VCSEL light sources for SS-OCT, a movable high-contrast grating (HCG) is used as the top mirror of the laser cavity, replacing the conventional distributed Bragg reflector mirror design. By applying a reverse bias voltage, the HCG mirror actuates downward toward the VCSEL cavity, changing the effective cavity length and resulting in wavelength tuning responses. The developed SS-OCT system allows an A-scan rate of 250 kHz, a detection sensitivity of 98 dB, and an axial imaging resolution of 22 µm (FWHM). The A-scan rate can be further improved to 500 kHz if both the backward (long to short wavelength) and forward laser sweep are used. In the experimental setup, a dual-channel acquisition scheme was utilized to provide calibration of the OCT signal with a separate calibration interferometer. Volumetric imaging of the human fingernail junction and mouse ear skin in vivo shows the feasibility of providing high speed imaging of the tissue architectures. In addition, utilizing the OCT angiography in combination with the variable interscan time analysis (VISTA) algorithm, it could provide subsurface volumetric microvascular imaging of the mouse ear skin with relative blood flow speed information. The MEMS tunable HCG-VCSEL light source can provide high-speed OCT and OCTA imaging with a more compact light source footprint and potentially a lower cost.

Keywords: MEMS, VCSEL, HCG, Wide tuning, High speed, High tuning speed, OCT, OCTA

1. INTRODUCTION

Optical coherence tomography (OCT) is a real-time and noninvasive imaging modality that enables micron scale, two-dimensional cross-sectional, and three-dimensional volumetric imaging of biological tissues and materials architecture [1]. OCT is measuring the echo time delay and magnitude of the reflected or backscattered light from the internal of the sample structures. SS-OCT has feasibility as ultrahigh speeds and high-resolution imaging modality in various clinical applications such as those related to cardiology [2], dermatology [3], ophthalmology [4], and gastroenterology diseases [5]. SS-OCT uses wavelength swept lasers and high speed analog to digital digitizer to achieve faster speeds and longer imaging ranges than spectral domain OCT [6]. High-speed SS-OCT is a rapidly emerging ophthalmologic technique with higher resolution than previous OCT techniques [7]. The key enabling component of this technique is a wavelength swept laser with a tuning range exceeding 70 nm and 100 kHz to 1+ MHz tuning repetition rate of the laser diode. The initial reports of this technique used optically-pumped MEMS-tunable VCSELs [7], which are considerably more costly, bulky, and complex to fabricate than conventional electrically-pumped VCSELs.

In the last decade, with the maturity of the wafer manfacturing and the micro-electromechanical systems developed, tunable vertical cavity surface emitting lasers (MEMS-VCSELs) have been adopted as a high performance swept source for SS-OCT, providing comprehensive adjustability of wide tuning range, high and tunable sweep speed, long dynamic coherence length, high output power, and wavelength flexibility. Although the optically-pumped MEMS-VCSEL light sources have been successfully demonstrated in the previous study [8]; however, the cost and reliability are significant drawbacks due to the complexity of device structures that require extra optical components, including the pump laser, the pump isolator, and the multiplexer, compared with the electrically-pumped MEMS-VCSELs. In this study, we revealed OCT imaging with a tunable HCG-VCSEL light source at the 1060 nm center wavelength. Furthermore, the OCT system parameters are shown in section 2.2. With this dual-channel SS-OCT system, we successfully demonstrated the OCT and OCTA image in section 3.

2. METHOD

2.1 Electrically pumped 1050 nm MEMS HCG-VCSELS

A widely and continuously tunable, electrically pumped VCSEL at 1060nm is used as the swept-source in the OCT system presented in this work [9, 10]. A key enabling technology in the wavelength-tunable VCSEL is the high-contrast grating (HCG) layer, which is used in place of a top DBR mirror in a conventional VCSEL. The HCG is integrated above an active region and bottom DBR mirror in a GaAs-based material system, as shown in Fig. 1(a). The HCG is a single layer of high refractive index material that exhibits high reflectivity across a wide tuning range of 100+ nm. An SEM image of the MEMS integrated HCG is shown in Fig. 1(b). By applying a reverse bias voltage between the p-DBR and suspended HCG, the HCG mirror actuates downwards towards the body of the VCSEL, changing the effective cavity length resulting in different wavelength tuning responses. Fig. 1(c) shows the emission wavelength of the tunable VCSEL biased at 4mA and 25C, as a function of tuning voltage from 10V to 24V. A single-mode, continuous wavelength tuning range of approximately 50 nm can be obtained. The VCSEL chip is packaged inside a standard TO56 package with a thermoelectric cooler for temperature control, and it is optically aligned to the HI1060 fiber pigtail using a conventional TOSA package assembly.

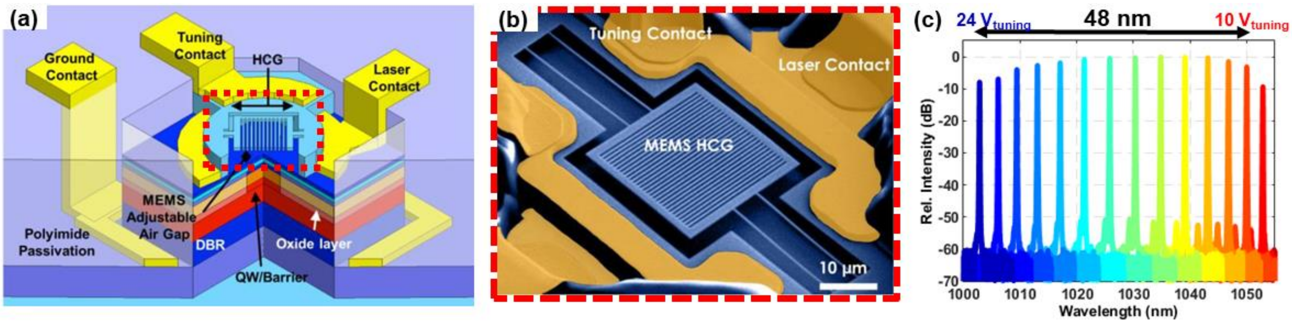

Figure 1. (a) Schematics of the MEMS tunable VCSEL at 1060nm. (b) A tilted view SEM image of the fabricated device, showing the MEMS HCG that can be actuated by voltage. (c) The measured emission wavelength of the MEMS tunable VCSEL as a function of tuning voltage from 10 to 24V.

2.2 Swept-Source OCT system setup

In this study, we use the arbitrary waveform generator (33250A, Agilent) to drive the VCSEL (BW10-1060-T-TO, Bandwidth10) with the 250 kHz sinusoidal wave function, and the VCSEL produces the sinusoidal and bidirectional wavelength sweeps, fringes from both the forward (short to long wavelength) and backward (long to short wavelength) sweeps were sampled, resulting in effective A-scan rates of 500 kHz; meanwhile, the synchronization trigger signal from the AFG transfers to the digitizer as the A-trigger signal. In this way, the continuous wavelength tuning range of 48 nm can be obtained shown in Fig. 3(a). The direct output power from the VCSEL is 250 µW; therefore, we amplify the power throughput to 30 mW by the booster optical amplifier (BOA1050S, Thorlabs).

Fig. 2 demonstrates the schematic of the 1060 nm swept-source OCT (SS-OCT) system, and it includes two modules, the Calibration interferometer (Calib.) and optical coherence tomography (OCT). The input light is separated into two lights by the 80/20 fiber-optic coupler, leading light into the OCT module. OCT module based on a Michelson interferometer comprising four fiber-optic couplers, each with a power split ratio of 50:50. In the sample arm, light exiting the fiber terminal was collimated using an achromatic lens (AC-080-016-C, Thorlabs) and subsequently deflected toward the sample surface by a pair of closely spaced galvanometer scanning mirrors (GVS102, Thorlabs). The use of an achromatic lens (AC-254-060-C, Thorlabs) as the focusing lens allowed for a lateral resolution of approximately 12.4 µm (full-width at half-maximum) based on resolution target (1951 USAF, Edmund) measurements. In the reference arm, to minimize the dispersion mismatch between the two arms, the same optics used in the sample arm, including the collimating lens and the focusing lens, was used except for the galvanometer scanner. Lastly, the backscattered light from both arms interfered at the 50/50 fiber-optic coupler, and the interference light signal was transferred into an electrical signal by the dual-balanced photodiode detector (PDB-482C-AC, Thorlabs). Before delivering the interference signals into the digitizer, the interference signals were filtered by the low-pass filter (BLP250+, Mini-circuits) with a 250-MHz 3-dB cutoff frequency to reduce high-frequency noise. The calibration interferometer module used the same optics and the electronics as well.

A high-speed digitizer (ATS9373, AlazarTech) with a 12-bit resolution was used for digitizing the detected OCT and Calib. signal into a digitized signal. An in-house developed graphical user interface based on C++ applied to control scanning patterns and data acquisition. Also, implement the GPU processing (CUDA Toolkit 10.2, Nvidia) to accelerate the data processing speed.

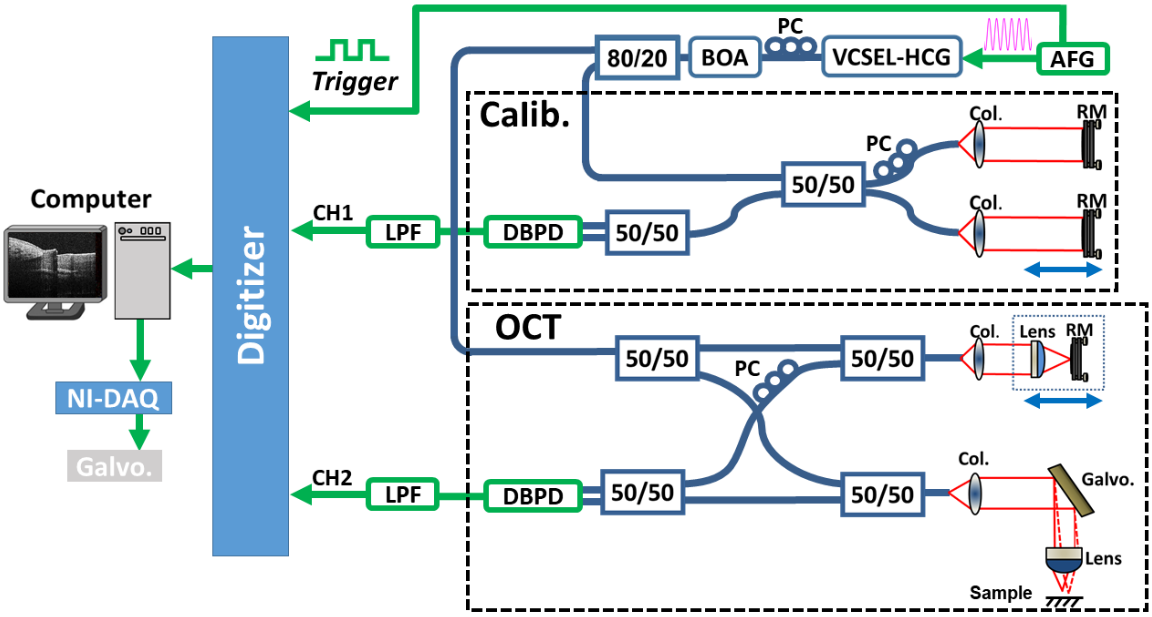

Fig. 2 Schematic of the swept-source optical coherence tomography (SS-OCT) system employed in this study. By using the dual channel acquisition, each A-scan calibrated and resampled by the calibration interferometer to overcome the lack of optical clock and enable higher performance; PC: polarization controller; Col: collimator; RM: reflection mirror; DBPD: dual-balanced photodetector; DAQ: data acquisition card; Galvo: galvanometer scanner; LPF: low pass filter; BOA: booster optical amplifier; AFG: arbitrary function generator; Calib: calibration interferometer.

2.3 Signal and imaging processing

OCT and Calib. interference fringes were digitized at 500 MSPS (12 bits ADC) with 1536 samples per sweep at 250 kHz A-scan rates. Since each sweep of the swept-source laser is not identical, it will cause errors in wavenumber sampling (non-linear). To calibrate for this sweep variation, we acquire every OCT fringe simultaneously with an Calib. fringe and compute a sample (time) to wavenumber (frequency) calibration for each A-scan. Then we resampled the OCT fringes to be linear in wavenumber using cubic-spline interpolation [11]. Background subtraction was applied to the unresampled fringes before the calibration. After the background subtraction and wavenumber calibration, we use the window function to shape the fringes before the Fourier transform, as depicted in Fig. 3(b).

OCT angiography image was calculated using a correlation mapping algorithm; this method has published by Chen et al [12]. To demonstrate OCTA, five repetitive B-scan frames were acquired at each location. Accordingly, each volumetric OCT raw data set includes 1600× 500 × 5 A-scans, where each B-scan frame consists of 1600 A-scans. After OCT images had been reconstructed from the raw data, the OCT images were used to compute the OCTA images; Furthermore, We also applied a variable interscan time analysis algorithm (VISTA). Since five repetitive frames were acquired per location, the OCTA interscan time could be adjusted or varied by changing the frame interval used to compute the OCTA images, enabling the differentiation of microvasculature with different blood flow rates, following the algorithm presented in previous published [13].

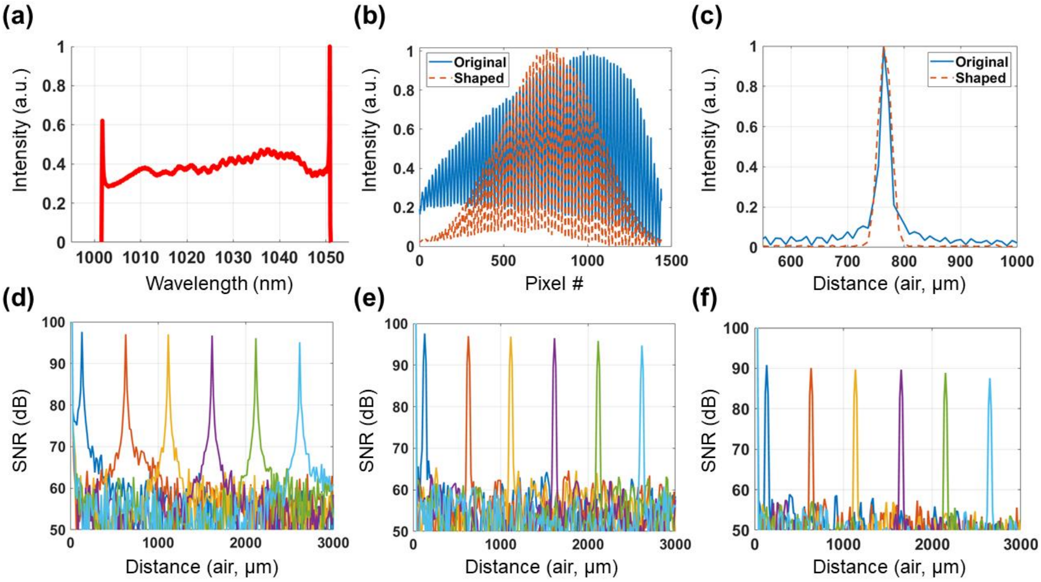

Fig. 3 (a) Measured wavelength sweep bandwidth at 250 kHz A-scan rate with the spectrum analyzer. (b) The OCT signal after calibrated by the calibration interference (blue) and filtered with the hamming filter (red). (c) Point spread function for 250 kHz A-scan rate, shown in logarithmic scale. (d) Backward sweeps corresponding sensitivity roll-off measurement in logarithmic scale. (e) Backward sweeps sensitivity roll-off measurement shaped with hamming filter in logarithmic scale. (f) the forward sweeps sensitivity roll-off measurement shaped with hamming filter in logarithmic scale.

3. RESULT

3.1 OCT image

Figure 4 illustrates volumetric OCT images of the fingernail junction and the tape (810 Scotch Tape, 3M). The imaging size is 5 mm x 5 mm; the images were acquired with the bidirectional sweeps 1060 nm OCT systems. Fig. 4(b) is the enface OCT image of the fingernail junction and presented with the backward sweep scanning result. The red line indicates the position of the cross-sectional image shown in (a), and (c) is the tape cross-sectional image. Then we presented the forward sweeps scanning result shown in Fig. 4(d, e, f), respectively. From Fig. 4(a, d), we can find the anatomy structure of the finger, including the epidermis (E), dermis (D), and proximal nail fold (PNF). Although the sensitivity of the forward sweeps is lower than backward sweeps, Fig. 4(d) still provides identical anatomic features of the finger, as shown in Fig. 4(a). Moreover, we mark and zoom in the upper layer with the ROI of each fingernail and tape cross-sectional images. Compared with the selected ROI in Fig. 4(a, d) and (c, f), Although there has a different sensitivity between backward and forward sweeps, both sweeps OCT images still provide a similar image quality.

Figure 5(a) illustrates the enface OCT image of the mouse ear, which was scanned by the backward sweeps, and the field of view (FOV) is the 5 mm x 5 mm; And Fig. 5(b) was a merged result of the bidirectional sweeps. First, we recomposed each B-scan (640*1600) by intersecting the backward and forward sweeps A-scan. After the re-composition, we marked the selection area with a blue square and compared it with the backward sweeps image marked with the yellow square. The marked area with the zoom-in image at the left-down side of Fig. 5(a, b); The merged OCT image has performed similar characteristics with the backward sweeps OCT image.

3.2 OCTA image

Figures 5(c) presents the maximum projected en face OCTA image with the OCT images collected with a frame rate and A-scan rate of 125 Hz and 250 kHz. The frame rate of 125 Hz corresponded to an OCTA interscan time of 8 ms. The number of A-scans per B-scan frame was set at 1,600. In the previous study [12], the longer OCTA interscan time allowed the detection of microvasculature with a relatively slower blood flow at the cost of being more vulnerable to the motion artifacts due to breathing. By computing the OCTA images with different OCTA interscan times based on the VISTA algorithm, as described previously [13], it provides relative blood flow information on the OCTA images, as depicted in Fig. 5(d), based on the OCTA images, as demonstrated in Figs. 5(c). The vessels with a larger diameter exhibited relatively faster blood flow than did those with smaller vessel diameters.

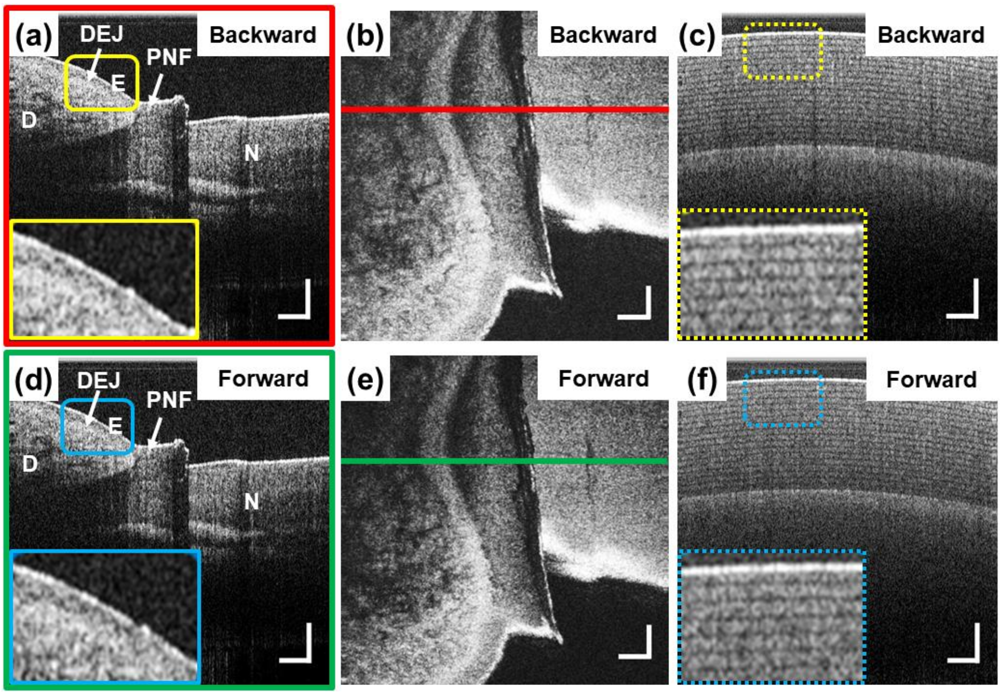

Fig. 4 (a) The backward sweeps scanning corss-sectional imaging result of the finger nail jution, and the location indicated with the red line in (b). (b) The enface finger nail junction image of the (a). (c) The backward sweeps scanning corss-sectional imaging result of the tape. (d) The forwardward sweeps scanning corss-sectional imaging result of the finger nail jution, and the location indicated with the green line in (e). (e) The enface finger nail junction image of the (d). (f) The forward sweeps scanning corss-sectional imaging result of the tape. D: dermis, DEJ: dermis and epidermis junction, E: epidermis, PNF: proximal nail folder. Scale bars: 500 µm.

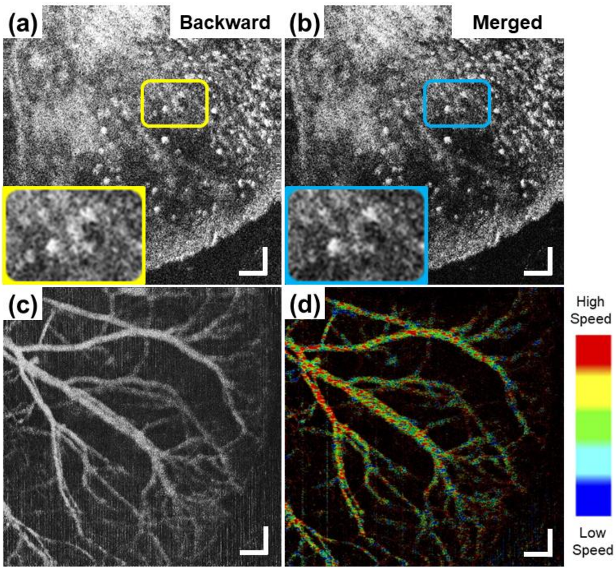

Fig. 5 (a) The backward sweeps enface OCT image of the mouse ear. (b) The bidirectional sweeps merged enface OCT image of the mouse ear. (c) En-face OCTA image of the mouse ear skin based on the maximum projection of the OCTA signals presented with the backward sweeps. (d) The backward sweeps reconstructed OCTA images with relative blood flow information obtained using the VISTA algorithm. Scale bars: 500 µm.

4. CONCLUSION

In summary, we present high speed, widely and continuously tunable, electrically-pumped VCSELs at 1060 nm wavelength center with a dual-channel SS-OCT system. With an HCG-based swept-source laser, we successfully presented the dermatology OCT image and the OCTA image of the mouse ear. This study is the first time that demonstrated the OCT image with the HCG VCSEL source. In addition, OCTA and VISTA imaging information further validated the sweep's stability of the HCG VCSEL. In the future, we will add the k-clock circuit into the HCG VCSEL module, and the OCT fringe can be real-time calibrated with the k-clock signal to reduce the processing cost of the processing unit to increase the frame rate. Also, we are working on the PS-OCT system construction to demonstrate the HCG VCSEL's polarization stability. With all these advantages, HCG-based tunable VCSELs are a prime candidate for enabling low-cost applications using tunable lasers in the OCT field.

ACKNOWLEDGMENT

The authors acknowledge the support from the Young Scholar Fellowship Program of the Ministry of Science and Technology (MOST) of Taiwan, Republic of China (ROC), (MOST-107-2636-E-002-003,108-2636-E-002-009, 109-2636-E-002-028 and 110-2636-E-002-025), National Taiwan University (NTU-IOTP-108PNTUS05 and NTU-IOTP-109PNTUS05), The authors also thank their cooperative partner Bandwidth10 in Taiwan for their advice and help in fabricating and testing the devices. Facility support was provided by the Molecular Imaging Center (MIC) at National Taiwan University. This article was subsidized by the Ministry of Science and Technology and National Taiwan University (NTU), Taiwan.

REFERENCES

[1] D. Huang, E. A. Swanson, C. P. Lin, J. S. Schuman, W. G. Stinson, W. Chang, M. R. Hee, T. Flotte, K. Gregory, C. A. Puliafito, and J. G. Fujimoto, "Optical Coherence Tomography," Science **254**, 1178-1181 (1991).

[2] G. J. Ughi, H. Wang, E. Gerbaud, J. A. Gardecki, A. M. Fard, E. Hamidi, P. Vacas-Jacques, M. Rosenberg, F. A. Jaffer, and G. J. Tearney, "Clinical Characterization of Coronary Atherosclerosis With Dual-Modality OCT and Near-Infrared Autofluorescence Imaging," JACC: Cardiovascular Imaging **9**, 1304-1314 (2016).

[3] J. Xu, S. Song, S. Men, and R. K. Wang, "Long ranging swept-source optical coherence tomography-based angiography outperforms its spectral-domain counterpart in imaging human skin microcirculations," Journal of Biomedical Optics **22**, 116007 (2017).

[4] S. Kishi, "Impact of swept source optical coherence tomography on ophthalmology," Taiwan Journal of Ophthalmology **6**, 58-68 (2016).

[5] T.-H. Tsai, C. Leggett, A. Trindade, A. Sethi, A.-F. Swager, V. Joshi, J. J. Bergman, H. Mashimo, N. Nishioka, and E. Namati, "Optical coherence tomography in gastroenterology: a review and future outlook," Journal of Biomedical Optics **22**, 121716 (2017).

[6] S. H. Yun, G. J. Tearney, J. F. de Boer, N. Iftimia, and B. E. Bouma, "High-speed optical frequency-domain imaging," Opt. Express **11**, 2953-2963 (2003).

[7] S. Ni, X. Wei, R. Ng, S. Ostmo, M. F. Chiang, D. Huang, Y. Jia, J. P. Campbell, and Y. Jian, "High-speed and widefield handheld swept-source OCT angiography with a VCSEL light source," Biomed. Opt. Express **12**, 3553-3570 (2021).

[8] V. Jayaraman, D. John, C. Burgner, M. Robertson, B. Potsaid, J. Jiang, T. Tsai, W. Choi, C. Lu, P. J. S. Heim, J. Fujimoto, and A. Cable, *Recent advances in MEMS-VCSELs for high performance structural and functional SS-OCT imaging* (SPIE, 2014).

[9] P. Qiao, K. T. Cook, K. Li, and C. J. Chang-Hasnain, "Wavelength-Swept VCSELs," IEEE Journal of Selected Topics in Quantum Electronics **23**, 1-16 (2017).
[10] M. C. Y. Huang, Y. Zhou, and C. J. Chang-Hasnain, "A surface-emitting laser incorporating a high-index-contrast subwavelength grating," Nature Photonics **1**, 119-122 (2007).
[11] B. Braaf, K. A. Vermeer, V. A. D. P. Sicam, E. van Zeeburg, J. C. van Meurs, and J. F. de Boer, "Phase-stabilized optical frequency domain imaging at 1-µm for the measurement of blood flow in the human choroid," Opt. Express **19**, 20886-20903 (2011).
[12] T.-H. Chen, Y.-C. Wu, T.-Y. Tsai, C.-B. Chueh, B.-H. Huang, Y.-P. Huang, M.-T. Tsai, Y. Yasuno, and H.-C. Lee, "Effect of A-scan rate and interscan interval on optical coherence angiography," Biomed. Opt. Express **12**, 722-736 (2021).
[13] S. B. Ploner, E. M. Moult, W. Choi, N. K. Waheed, B. Lee, E. A. Novais, E. D. Cole, B. Potsaid, L. Husvogt, J. Schottenhamml, A. Maier, P. J. Rosenfeld, J. S. Duker, J. Hornegger, and J. G. Fujimoto, "TOWARD QUANTITATIVE OPTICAL COHERENCE TOMOGRAPHY ANGIOGRAPHY: Visualizing Blood Flow Speeds in Ocular Pathology Using Variable Interscan Time Analysis," RETINA **36**, S118-S126 (2016).